

**Polyhedral plasmonic nanoclusters through multi-step colloidal chemistry**

Journal:	<i>Materials Horizons</i>
Manuscript ID	MH-COM-08-2020-001311.R1
Article Type:	Communication
Date Submitted by the Author:	19-Oct-2020
Complete List of Authors:	Tanjeem, Nabila; Harvard University, School of Engineering and Applied Sciences Chomette, Cyril; ICMCB, Schade, Nicholas; University of Chicago, James Franck Institute; Harvard University, Physics Ravaine, Serge; CRPP Duguet, Etienne; Univ. Bordeaux, ICMCB/CNRS Tréguer-Delapierre, Mona; Institut de Chimie de la Matière Condensée de Bordeaux Manoharan, Vinothan; Harvard University, Department of Physics

POLYHEDRAL PLASMONIC NANOCCLUSERS THROUGH MULTI-STEP COLLOIDAL CHEMISTRY

NABILA TANJEEM, CYRIL CHOMETTE, NICHOLAS B. SCHADE, SERGE RAVAINÉ,
ETIENNE DUGUET, MONA TRÉGUER-DELAPIERRE, AND VINOTHAN N.
MANOHARAN

New concepts statement

We demonstrate a new concept for making nanostructures. In research and industry, molecules from drugs to polymers are made by combining high-yield chemical reactions in series. We extend this approach to the nanoscale: we make *metamolecules* by combining high-yield *colloidal* reactions. Metamolecules are highly symmetric nanoclusters of metal and dielectric. They are needed for exotic optical materials like metafluids, but they are notoriously difficult to make because of the precision required. We address this challenge by combining inorganic growth, polymerization, and metal deposition. Though no individual reaction is new, the way we combine them is – much as the novelty in an organic synthesis scheme lies in determining what series of reactions will yield a target molecule. Through painstaking single-cluster spectroscopy measurements and comparison to simulation, we show that the morphology is controlled to nanometer-scale precision. Previous approaches to making metamolecules fall into two classes: lithography, which offers control over morphology but limited throughput, and self-assembly, which offers high precision but limited control over yield. Our approach fits into neither category, yet offers the best of both: high precision, high morphology yield, and bulk scale-up. It can be adapted to many other material systems.

Cite this: DOI: 00.0000/xxxxxxxxxx

Polyhedral plasmonic nanoclusters through multi-step colloidal chemistry[†]

Nabila Tanjeem,^{‡,a} Cyril Chomette,^{‡,b} Nicholas B. Schade,^c Serge Ravaine,^d Etienne Duguet,^{*,b} Mona Tréguer-Delapierre,^{*,b} and Vinodhan N. Manoharan^{*,a,c}

Received Date

Accepted Date

DOI: 00.0000/xxxxxxxxxx

We describe a new approach to making plasmonic metamolecules with well-controlled resonances at optical wavelengths. Metamolecules are highly symmetric, subwavelength-scale clusters of metal and dielectric. They are of interest for metafluids, isotropic optical materials with applications in imaging and optical communications. For such applications, the morphology must be precisely controlled: the optical response is sensitive to nanometer-scale variations in the thickness of metal coatings and the distances between metal surfaces. To achieve this precision, we use a multi-step colloidal synthesis approach. Starting from highly monodisperse seeds, we grow octahedral clusters of polymer spheres using seeded-growth polymerization. We then overgrow the silica and remove the polystyrene to create a dimpled template. Finally, we attach six silica satellites to the template and coat them with gold. Using single-cluster spectroscopy, we show that the plasmonic resonances are reproducible from cluster to cluster. By comparing the spectra to theory, we show that the multi-step synthesis approach can control the distances between metallic surfaces to nanometer-scale precision. More broadly, our approach shows how metamolecules can be produced in bulk by combining different, high-yield colloidal synthesis steps, analogous to how small molecules are produced by multi-step chemical reactions.

Fabricating plasmonic building blocks (or “metamolecules”) for

optical metamaterials^{1–3} requires precise positioning of metal and dielectric. The optical response is sensitive to nanometer-scale variations in both the thickness of metal coatings and the distances between metal surfaces. To date, two general approaches have been developed to create such structures: lithography, in which metal and dielectric are patterned and deposited stepwise^{4–8}, and self-assembly, in which nanoparticles form nanoclusters, driven by DNA-mediated^{9,10} or capillary interactions^{11,12}. Lithography offers precise control over morphology but limited throughput. Self-assembly driven only by electrostatic, DNA-mediated, or capillary interactions offers high precision but limited control over yield.

Here we demonstrate a third approach that is based on neither lithography nor self-assembly: multi-step colloidal synthesis. We focus on the creation of nanoclusters with octahedral symmetry because their high symmetry may prove useful in metafluids^{13–15}. We first synthesize a silica template with octahedrally-coordinated “dimples”^{16,17}, as shown in steps 1–4 of Fig. 1. This method takes advantage of several high-yield synthetic steps: a multi-stage silica-particle synthesis process¹⁸ that results in seed particles with a polydispersity index of only 1.002 (see ESI sec. 1.1); the templated synthesis of polystyrene colloidal molecules¹⁹, which results in octahedral clusters with a yield as high as 80%^{18,20}; the overgrowth of the silica core followed by removal of the polystyrene spheres¹⁶; and the regioselective functionalization of the resulting concave dimples in the silica.

The challenge is to attach metal to the resulting functionalized, dimpled, octahedrally symmetric silica particles such that the distance between metal surfaces is controlled to nanometer-scale precision. In self-assembly approaches, this precision can be achieved by functionalizing gold nanoshells with a self-assembled monolayer and clustering them with capillary forces^{11,12}, but this method yields clusters with many different morphologies. Another self-assembly approach involves attaching DNA-functionalized gold nanoparticles to DNA origami templates¹⁰. This method also leads to precise control over the separation dis-

^a Harvard John A. Paulson School of Engineering and Applied Sciences, Harvard University, Cambridge, MA 02138, USA.

^b Univ. Bordeaux, CNRS, ICMCB, UMR5026, F-33608 Pessac, France.

^c Department of Physics, Harvard University, Cambridge, MA 02138, USA.

^d Univ. Bordeaux, CNRS, CRPP, UMR5031, F-33608 Pessac, France.

* To whom correspondence should be addressed: etienne.duguet@icmcb.cnrs.fr, mona.treguer@icmcb.cnrs.fr, vnm@seas.harvard.edu

[†] Electronic Supplementary Information (ESI) available: [details of any supplementary information available should be included here]. See DOI: 00.0000/00000000.

[‡] These authors contributed equally to this work.

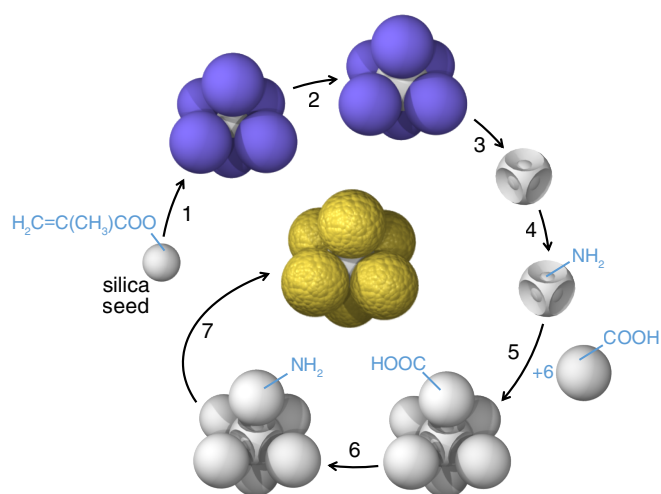


Fig. 1 Our synthesis scheme for plasmonic clusters consists of seven steps: (1) Seeded-growth emulsion polymerization of styrene on spherical silica particles with a diameter of 86 nm; (2) overgrowing the silica seed and (3) dissolving polystyrene, which results in structures with six concave dimples; (4) aminating the residual polystyrene at the bottom of the dimples to complete the template; (5) locking carboxylated silica nanospheres with a diameter of 137 nm onto the aminated dimples; (6) converting the carboxylate groups on the silica satellites into amine groups; (7) growing a thin gold shell on the spheres by the site-specific adsorption of gold nuclei and subsequent regrowth. See ESI sec. 1.1–1.4 for details on the synthesis.

tance, but it produces clusters with different numbers of particles and morphologies.

By contrast, the dimpled templates offer a highly consistent morphology, but until now no approach has led to precise control over the separation distance. In previous work, gold satellites were grown directly on the dimpled templates²¹. This approach requires iterative growth and oxidative etching of the gold, which results in the satellites varying in size and shape. Hence the inter-particle distances were not well controlled. In the present study, we first attempted to lock pre-synthesized, highly monodisperse, ultra-smooth gold spheres²² to the dimples, but we obtained a low yield of clusters with six particles attached, perhaps because of the large density difference between silica and gold.

Therefore, instead of attaching gold directly to the dimples, we pursue a multi-step approach, as shown in steps 5–7 of Fig. 1. We first attach silica spheres to the dimples and then grow a gold layer on top of them. We lock highly monodisperse silica particles (polydispersity index 1.001) onto the dimples, building on a previously developed recipe²³. This recipe takes advantage of the PS molecules that are grafted to the silica particles in step 1 and that remain after dissolution of the PS spheres in step 3. The chains are aminated and then coupled to carboxylated silica particles through a peptide reaction in dimethyl formamide. The solvent allows the aminated PS chains to extend, facilitating the capture of the particles by the dimples. To fill all the dimples, we use a large excess of silica particles (400:1). Then we use a seeded-growth method²⁴ to grow a gold film of controlled thickness on

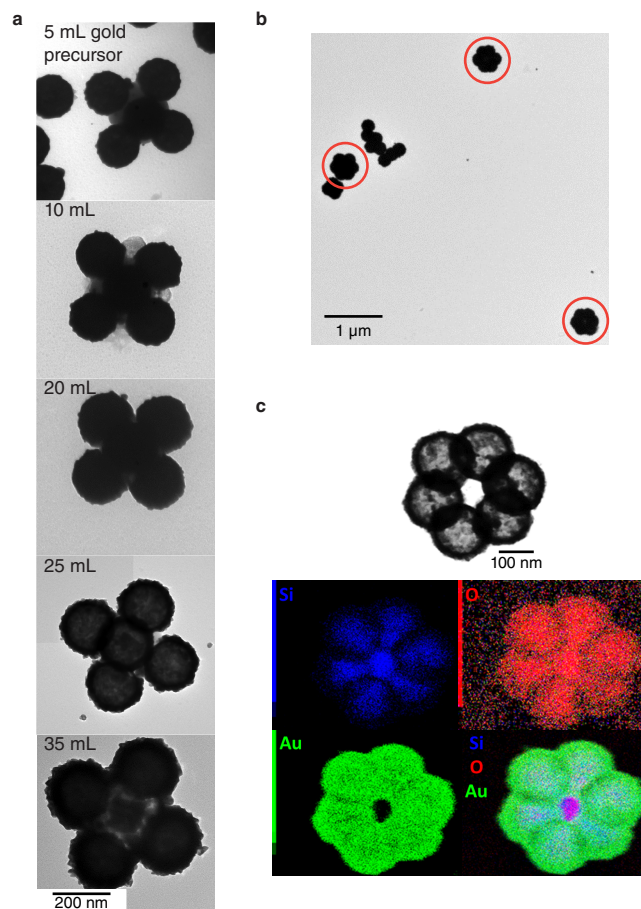


Fig. 2 Electron microscopy shows the geometry of the nanoclusters. **a**, TEM images of silica/gold clusters with varying gold shell thicknesses, obtained with different amounts of gold precursor, from 5–35 mL. **b**, TEM image of clusters obtained for the regrowth condition of 25 mL gold precursor. Octahedral clusters are circled in red. Other particles are unattached gold nanoshells, which are formed when the excess silica particles added in step 4 of Fig. 1 are functionalized and coated with gold. Drying the sample for TEM imaging can cause these particles to aggregate. **c**, STEM-EDX elemental mapping of an octahedral cluster: bright field TEM image (top) and silicon, oxygen, gold, and superimposed EDX maps evidence the core-shell morphology of the six satellites. See ESI sec. 1.5 for details on the characterization methods.

the silica. Growth occurs only on the silica satellites and not the central particle because the satellites are functionalized with carboxyl groups, which we can selectively convert to amine groups prior to gold plating. Gold seeds do not attach to the central particle because it is hydrophobic (ESI sec. 1.2.1). Thus, we control the separation distance by taking advantage of the very low polydispersity of the silica synthesis reaction^{18,25} and the precision of the seeded-growth gold plating technique. Furthermore, because the silica core size and gold shell thickness can be changed independently, this approach provides independent control over the two geometrical features that control the frequency of the plasmon resonances: the separation distance and the separation-to-diameter ratio²⁶.

Transmission electron microscopy (TEM) shows that the synthesis is successful. As shown in Fig. 2a, we control the thickness of the gold shell by changing the amount of gold precursor in the

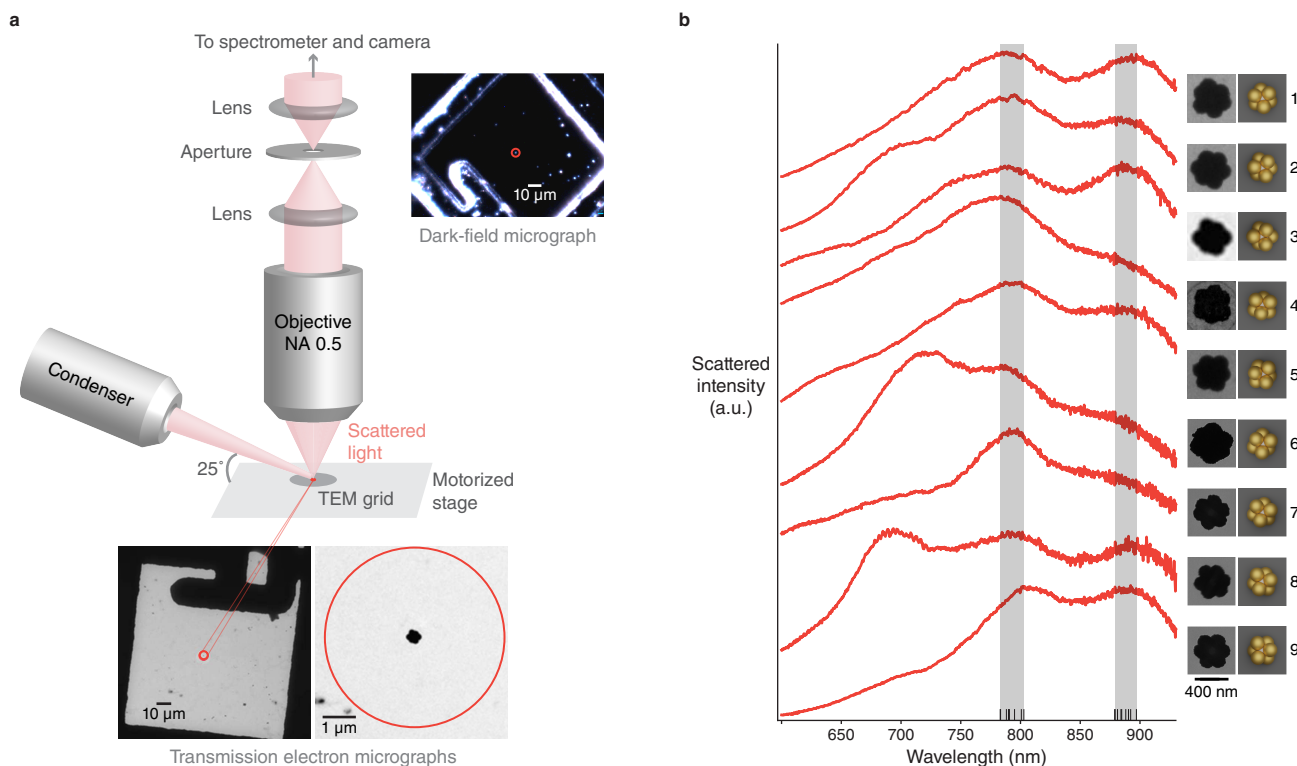


Fig. 3 Single-cluster spectroscopy shows that individual clusters have two consistent peaks. **a**, Illustration of setup for measuring scattering spectra of individual nanoclusters (ESI sec. 1.5). An unpolarized halogen lamp illuminates the sample, and an objective (NA = 0.5) collects the scattered light from a spot 1 μm in diameter, set by the aperture. TEM images show a cluster near marker “P” on the finder grid at low and high magnification. Dark-field micrograph, obtained from the setup, shows the same cluster. **b**, Measured spectra of nine individual octahedral clusters. Each spectrum is accompanied by a TEM image of the measured cluster and a 3D rendering showing its approximate orientation. Upward ticks on the wavelength axis show the peak positions. Gray regions denote the range of these positions. Cluster 3 is also shown in the micrographs of **a**.

synthesis step. We find that for a shell thickness of about 25 nm, the geometry remains consistent from cluster to cluster (Fig. 2b). Elemental mapping using energy-dispersive X-ray analysis (EDX) shows that the gold layer is specifically deposited on each of the six silica satellites, while the central silica particle remains gold-free (Fig. 2c).

Because the gold shells are separated by only a few nanometers, too small to measure precisely with TEM, we infer the separation distances and their variation using single-cluster spectroscopy and simulation. The plasmon resonances provide the most stringent test of the precision of our technique because they are sensitive to small changes in the separation¹³. We first locate isolated octahedral clusters on a marked grid using TEM, then transfer the TEM grid to a microscope stage. We set the illumination angle such that the objective collects the scattered light only. After finding the same nanoclusters in this dark-field setup, we measure the spectrum of light scattered from each individual cluster using a spectrometer attached to the microscope. The setup and representative images are shown in Fig. 3a.

Each of the nine clusters we measure shows two major peaks, one at $791.5 \pm 6.5 \text{ nm}$, another at $886.2 \pm 5.9 \text{ nm}$ (Fig. 3b). We identify the peak positions by searching for the local maxima in the spectra, which can be located precisely, despite the width of the peaks. The uncertainties represent one standard deviation

about the mean of the peak positions of the nine spectra. Whereas the microscope images confirm that each nanocluster has octahedral symmetry and that the number and approximate positions of the core-shell particles are consistent from cluster to cluster, the small uncertainty in peak positions suggests that the separation distance is also consistent. To make a quantitative statement about how precisely this distance is controlled, we first use simulation to determine the origins of the resonances, then explore how changing the separation distance affects the resonances.

To understand the origin of the scattering peaks, we use finite-difference time-domain (FDTD) simulations. Our simulations account for the experimental setup (Figs. 4a and S1)—including the substrate and the numerical aperture of the lens—and the geometry of the nanoclusters (Figs. 4b and S2)—including the fact that the shells terminate at the surface of the central particle. We first estimate the positions of the particles and the interparticle separations from TEM images, then refine these values to obtain agreement between simulation and experiment. We find that the simulation reproduces the peaks in the experimental spectra when the interparticle separation is 2 nm (Fig. 4c).

By mapping the charge density in the simulations (Fig. 4c) and calculating the far-field radiation pattern at different wavelengths (Fig. S4), we find that the peak near 900 nm originates from an electric dipolar resonance, and the peak near 800 nm has an elec-

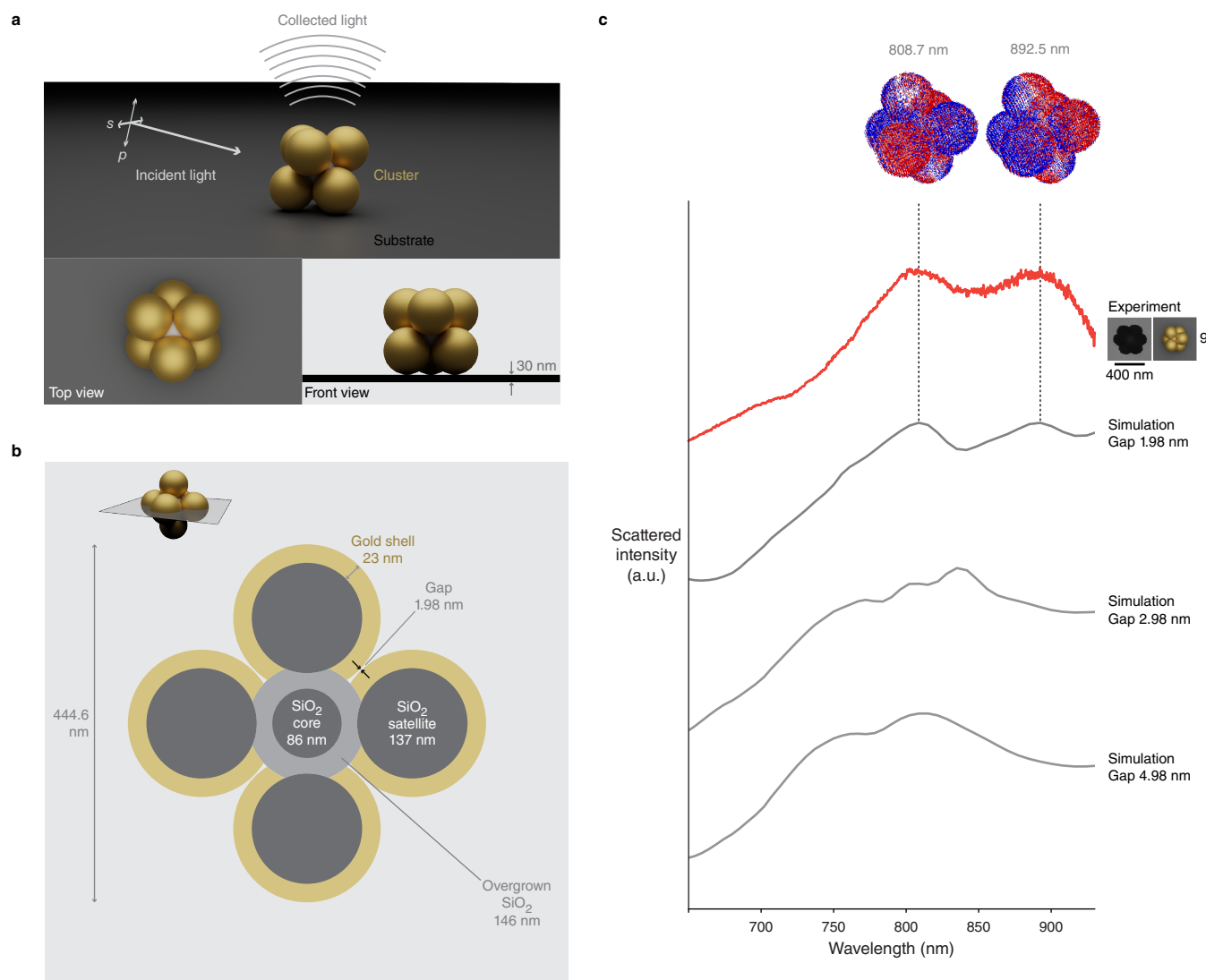


Fig. 4 Finite-difference time-domain (FDTD) simulations reproduce the locations of the measured peaks. **a**, Illustration of simulation geometry, showing 3D renderings of a scale model of a cluster, with perspective, top, and front views. The simulation accounts for the incidence angle, collection angle, and substrate in the experiments (ESI sec. 2). To mimic an unpolarized light source, we add the scattered intensity from two orthogonal polarizations, shown as s and p . **b**, Schematic of cross-section of an octahedral cluster, showing length scales used in the simulation. “Gap” refers to the separation distance between the gold shells. **c**, Spectra from simulation (gray curves) and experiment (red curve, corresponding to cluster 9 of Fig. 3b). The spectrum simulated at a gap size of 2 nm (top gray curve) reproduces the locations of the peaks in the measured spectrum. Increasing the gap by 1 nm or more in the simulation shifts the two peaks to wavelengths that are outside the range of the observations. Charge density maps at 808.7 and 892.5 nm show different resonant modes at the two peaks. See Fig. S3 for polarized spectra.

tric quadrupolar component. The simulation does not explain all the features of the spectra. The peak close to 700 nm—which appears in three of the nine spectra and corresponds to the electric quadrupolar resonance (Fig. S4)—and the variation in the heights of the main two peaks likely arise from roughness in the gold shells. Because this roughness is comparable to the gap between the shells, we expect the relative magnitudes of the dipolar and higher-order resonances to depend sensitively on the details of the topography in the gap^{27–29}.

With this understanding of the peak origins, we examine how changing the separation distance affects the locations of the resonances. Previous theoretical studies have shown that the dipolar resonances in a tetrahedral cluster are sensitive to the ratio of the

inter-particle separation distance to particle diameter¹³. When this ratio changes from 0.02 to 0.04, the electric dipolar resonance shifts by about 100 nm. From the separation estimated with TEM (2–5 nm) and the overall diameter of the core-shell geometry, we estimate that the separation-to-diameter ratio of our octahedral cluster is between 0.011 and 0.027. Within this range, we expect the resonance peaks to be at least as sensitive as those in the previous study¹³.

We use our simulation to confirm this sensitivity. By changing the inter-particle separation from 2 nm (shell thickness 23 nm, diameter $137 + 46 = 183$ nm, separation-to-diameter ratio 0.011) to 5 nm (shell thickness 21.5 nm, diameter $137 + 43 = 180$ nm, separation-to-diameter ratio 0.022), the dipolar peak blue-shifts

about 90 nm (Fig. 4c) and the higher-order peak blue-shifts about 50 nm. The uncertainty in peak positions from experimental measurements is an order of magnitude smaller, 5.9 nm for the dipolar peak and 6.5 nm for the higher-order peak. By assuming a linear relationship between peak positions and interparticle separations, we obtain a conservative estimate for the uncertainty in interparticle separation: 0.2–0.4 nm. In other words, if the gap varied by more than this amount from cluster to cluster, the simulated spectra would not match the data. From this result, we conclude that the multi-step synthesis approach can control the interparticle separation to nanometer precision.

To be clear, “nanometer precision” refers to the average distance between the gold layers on the silica satellites. As can be seen in Fig. 2a, the gold layers have a roughness that is larger than a nanometer. This roughness might contribute to the observed variation in amplitude of the peaks from cluster to cluster. However, the consistency of the peak positions indicates that the average separation distance is very well controlled. In previous measurements on individual nanoclusters^{30,31}, the spectra varied from cluster to cluster. This variation can lead to spectral broadening in bulk measurements^{32,33}, which might be avoided by using clusters made with our approach.

We estimate the morphology yield to be 60%, based on analysis of electron microscopy images at different steps along the synthesis pathway shown in Fig. 1. The yield of seed silica particles with octahedrally-coordinated polystyrene satellites (step 1) is 62% (total clusters counted $N \approx 100$), with the side products being silica cores with three, four, and five polystyrene satellites (Table S1). After overgrowth of the silica core (step 2) and removal of the polystyrene spheres (step 3), the yield of silica cores with octahedrally coordinated dimples is 60% ($N \approx 100$, Table S2). After functionalizing the dimples (step 4) and adding silica satellites in large excess (step 5), we observe that nearly all of the dimples are filled. Finally, after functionalizing the silica satellites (step 6) and growing gold shells on them (step 7), we find that 60% ($N = 25$) of the resulting clusters have six gold shells attached to a central silica particle (Table S3). These results show that the step that limits the yield is likely the synthesis of octahedral silica/polystyrene colloidal molecules (step 1). Previous work^{18,20} has shown that the yield of this step can be increased to more than 80%. We note also that because each step of the synthesis is done in bulk, the procedure can be scaled up to produce clusters at gram scales or more.

Future work might extend this approach to produce other plasmonic metamolecules¹³. To this end, one can control the morphology by changing the dimple geometry of the overgrown silica; by tuning the core size, it is possible to make tetrahedral and dodecahedral geometries^{16,34}. Also, because the core size, shell thickness, and interparticle separation can be controlled independently of one another, there are many ways to tune the positions of the plasmon resonances.

More generally, our method illustrates the degree to which colloidal morphology can now be controlled through chemistry. The precision of our method stems from the versatility of seeded-growth reactions. These are used to create the highly monodisperse silica particles for the core and satellites, to control the

thickness of the gold films (step 7 of Fig. 1), to overgrow the silica core (step 2), and to make the octahedral cluster of sacrificial polymer particles that coordinate the central silica core (step 1). The reaction in step 1 relies on a geometrical effect³⁵ that results in a narrow distribution of numbers of particles attached to a central core, even when the initial seeds of those particles are randomly distributed on the core surface³⁶. A similar process in which spheres adsorb onto a central core—rather than grow on it—is the basis of a recent synthesis method for making patchy colloidal particles with controlled morphology³⁷. Like our method, this method uses multiple high-yield synthesis steps to produce large quantities of specific clusters. Such schemes, which resemble the multi-step synthetic schemes used to produce complex molecules from organic reagents, represent a new and emerging paradigm in colloidal materials. They have clear advantages over self-assembly and lithography: they can produce bulk quantities of complex three-dimensional structures in bulk with no annealing required. Our results demonstrate that the multi-step approach can meet even the most stringent requirements for precision over the assembly.

Conflicts of interest

There are no conflicts to declare.

Acknowledgments

We thank Arthur McClelland for help with the dark-field spectroscopy setup, Carolyn Marks and Adam Graham for help with TEM, and Sarah Kostinski for helpful discussions about the simulation. Some of the TEM experiments were performed at the Bordeaux Imaging Center and Plateforme de Caractérisation des Matériaux of the University of Bordeaux. We gratefully acknowledge Jérôme Majimel for his assistance in mapping analysis. This work was supported by the LabEx AMADEus (ANR-10-LABX-42) and IdEx Bordeaux (ANR-10-IDEX-03-02), that is, the Investissements d’Avenir programme of the French government managed by the Agence Nationale de la Recherche. The research was partially supported by the National Science Foundation through the Harvard University Materials Research Science and Engineering Center under grant number DMR-2011754. This work was performed in part at the Center for Nanoscale Systems (CNS), a member of the National Nanotechnology Coordinated Infrastructure Network (NNCI), which is supported by the National Science Foundation under NSF award no. 1541959. CNS is part of Harvard University.

Notes and references

- 1 C. M. Soukoulis and M. Wegener, *Nature Photonics*, 2011, **5**, 523–530.
- 2 V. M. Shalaev, W. Cai, U. K. Chettiar, H.-K. Yuan, A. K. Sarychev, V. P. Drachev and A. V. Kildishev, *Optics Letters*, 2005, **30**, 3356–3358.
- 3 S. Gomez-Graña, A. L. Beulze, M. Treguer-Delapierre, S. Mornet, E. Duguet, E. Grana, E. Cloutet, G. Hadziioannou, J. Leng, J.-B. Salmon, V. G. Kravets, A. N. Grigorenko, N. A. Peyyety, V. Ponsinet, P. Richetti, A. Baron, D. Torrent and P. Barois, *Materials Horizons*, 2016, **3**, 596–601.
- 4 N. Liu, H. Guo, L. Fu, S. Kaiser, H. Schweizer and H. Giessen, *Nature Materials*, 2008, **7**, 31–37.
- 5 M. Decker, R. Zhao, C. M. Soukoulis, S. Linden and M. Wegener, *Optics Letters*, 2010, **35**, 1593–1595.
- 6 J. Valentine, S. Zhang, T. Zentgraf, E. Ulin-Avila, D. A. Genov, G. Bartal and X. Zhang, *Nature*, 2008, **455**, 376–379.

- 7 M. S. Rill, C. Plet, M. Thiel, I. Staude, G. von Freymann, S. Linden and M. Wegener, *Nature Materials*, 2008, **7**, 543–546.
- 8 D. B. Burckel, J. R. Wendt, G. A. T. Eyck, J. C. Ginn, A. R. Ellis, I. Brener and M. B. Sinclair, *Advanced Materials*, 2010, **22**, 5053–5057.
- 9 E.-M. Roller, L. K. Khorashad, M. Fedoruk, R. Schreiber, A. O. Govorov and T. Liedl, *Nano Letters*, 2015, **15**, 1368–1373.
- 10 J. Lee, J.-H. Huh, K. Kim and S. Lee, *Advanced Functional Materials*, 2018, **28**, 1707309.
- 11 J. A. Fan, C. Wu, K. Bao, J. Bao, R. Bardhan, N. J. Halas, V. N. Manoharan, P. Nordlander, G. Shvets and F. Capasso, *Science*, 2010, **328**, 1135–1138.
- 12 J. A. Fan, K. Bao, L. Sun, J. Bao, V. N. Manoharan, P. Nordlander and F. Capasso, *Nano Letters*, 2012, **12**, 5318–5324.
- 13 Y. A. Urzhumov, G. Shvets, J. Fan, F. Capasso, D. Brandl and P. Nordlander, *Optics Express*, 2007, **15**, 14129–14145.
- 14 A. Alù and N. Engheta, *Optics Express*, 2009, **17**, 5723–5730.
- 15 K. Kim, S. Yoo, J.-H. Huh, Q.-H. Park and S. Lee, *ACS Photonics*, 2017, **4**, 2298–2311.
- 16 A. Désert, C. Hubert, Z. Fu, L. Moulet, J. Majimel, P. Barboteau, A. Thill, M. Lansalot, E. Bourgeat-Lami, E. Duguet and S. Ravaine, *Angewandte Chemie International Edition*, 2013, **52**, 11068–11072.
- 17 C. Hubert, C. Chomette, A. Désert, M. Sun, M. Tréguer-Delapierre, S. Mornet, A. Perro, E. Duguet and S. Ravaine, *Faraday Discussions*, 2015, **181**, 139–146.
- 18 A. Désert, I. Chaduc, S. Fouilloux, J.-C. Taveau, O. Lambert, M. Lansalot, E. Bourgeat-Lami, A. Thill, O. Spalla, S. Ravaine and E. Duguet, *Polymer Chemistry*, 2012, **3**, 1130–1132.
- 19 A. Perro, E. Duguet, O. Lambert, J. C. Taveau, E. Bourgeat-Lami and S. Ravaine, *Angewandte Chemie International Edition*, 2009, **121**, 367–371.
- 20 A. Désert, J. Morele, J.-C. Taveau, O. Lambert, M. Lansalot, E. Bourgeat-Lami, A. Thill, O. Spalla, L. Belloni, S. Ravaine and E. Duguet, *Nanoscale*, 2016, **8**, 5454–5469.
- 21 C. Chomette, M. Tréguer-Delapierre, N. B. Schade, V. N. Manoharan, O. Lambert, J.-C. Taveau, S. Ravaine and E. Duguet, *ChemNanoMat*, 2017, **3**, 160–163.
- 22 Y.-J. Lee, N. B. Schade, L. Sun, J. A. Fan, D. R. Bae, M. M. Mariscal, G. Lee, F. Capasso, S. Sacanna, V. N. Manoharan and G.-R. Yi, *ACS Nano*, 2013, **7**, 11064–11070.
- 23 P.-E. Rouet, C. Chomette, E. Duguet and S. Ravaine, *Angewandte Chemie International Edition*, 2018, **57**, 15754–15757.
- 24 S. J. Oldenburg, R. D. Averitt, S. L. Westcott and N. J. Halas, *Chemical Physics Letters*, 1998, **288**, 243–247.
- 25 K. D. Hartlen, A. P. T. Athanasopoulos and V. Kitaev, *Langmuir*, 2008, **24**, 1714–1720.
- 26 P. K. Jain and M. A. El-Sayed, *The Journal of Physical Chemistry C*, 2007, **111**, 17451–17454.
- 27 J. B. Lassiter, J. Aizpurua, L. I. Hernandez, D. W. Brandl, I. Romero, S. Lal, J. H. Hafner, P. Nordlander and N. J. Halas, *Nano Letters*, 2008, **8**, 1212–1218.
- 28 P. S. Popp, J. F. Herrmann, E.-C. Fritz, B. J. Ravoo and C. Höppener, *Small*, 2016, **12**, 1667–1675.
- 29 S. Oikawa, H. Minamimoto, A. Ohnuki and K. Murakoshi, *Nanoscale*, 2020, **12**, 11593–11600.
- 30 A. S. Urban, X. Shen, Y. Wang, N. Large, H. Wang, M. W. Knight, P. Nordlander, H. Chen and N. J. Halas, *Nano Letters*, 2013, **13**, 4399–4403.
- 31 K. J. Park, J.-H. Huh, D.-W. Jung, J.-S. Park, G. H. Choi, G. Lee, H.-G. Park, G.-R. Yi and S. Lee, *Scientific Reports*, 2017, **7**, 6045.
- 32 S. N. Sheikholeslami, H. Alaeian, A. L. Koh and J. A. Dionne, *Nano Letters*, 2013, **13**, 4137–4141.
- 33 Z. Qian, S. P. Hastings, C. Li, B. Edward, C. K. McGinn, N. Engheta, Z. Fakhraai and S.-J. Park, *ACS Nano*, 2015, **9**, 1263–1270.
- 34 V. Many, R. Dézert, E. Duguet, A. Baron, V. Jangid, V. Ponsinet, S. Ravaine, P. Richetti, P. Barois and M. Tréguer-Delapierre, *Nanophotonics*, 2019, **8**, 549–558.
- 35 N. B. Schade, M. C. Holmes-Cerfon, E. R. Chen, D. Aronzon, J. W. Collins, J. A. Fan, F. Capasso and V. N. Manoharan, *Physical Review Letters*, 2013, **110**, 148303.
- 36 A. Thill, A. Désert, S. Fouilloux, J.-C. Taveau, O. Lambert, M. Lansalot, E. Bourgeat-Lami, O. Spalla, L. Belloni, S. Ravaine and E. Duguet, *Langmuir*, 2012, **28**, 11575–11583.
- 37 Z. Gong, T. Hueckel, G.-R. Yi and S. Sacanna, *Nature*, 2017, **550**, 234–238.